scientific reports

Check for updates

OPEN

Usage of computational method for hemodynamic analysis of intracranial aneurysm rupture risk in different geometrical aspects

Mehdi Fattahi[1,2], Seyyed Amirreza Abdollahi[3]✉, Ali Hosin Alibak[4], Saleh Hosseini[5]✉ & Phuyen Dang[1,2]

The importance of the parent vessel geometrical feature on the risk of cerebral aneurysm rupture is unavoidable. This study presents inclusive details on the hemodynamics of Internal carotid artery (ICA) aneurysms with different parent vessel mean diameters. Different aspects of blood hemodynamics are compared to find a reasonable connection between parent vessel mean diameter and significant hemodynamic factors of wall shear stress (WSS), oscillatory shear index (OSI), and pressure distribution. To access hemodynamic data, computational fluid dynamics is used to model the blood stream inside the cerebral aneurysms. A hemodynamic comparison of the selected cerebral aneurysm shows that the minimum WSS is reduced by about 71% as the parent vessel's mean diameter is increased from 3.18 to 4.48 mm.

Endovascular coiling is a minimally invasive technique used to treat intracranial aneurysms and reduce the risk of rupture. It involves inserting small metal coils into the aneurysm sac, promoting thrombosis (blood clotting) and reducing blood flow into the aneurysm. The coiling procedure has several effects on the hemodynamics of the aneurysm, contributing to the reduction in rupture risk. Here are some ways in which endovascular coiling influences hemodynamics and reduces aneurysm rupture risk[1–3].

Coiling disrupts the normal blood flow patterns within the aneurysm by filling the sac with coils. This promotes flow diversion away from the aneurysm, reducing the impact of high-velocity jets and flow impingement on the vulnerable aneurysm wall. By redirecting blood flow, coiling helps alleviate the hemodynamic stress that can lead to aneurysm rupture[4–6].

The coils placed within the aneurysm initiate thrombosis, leading to the formation of a blood clot. As the clot matures and organizes, it further reduces blood flow into the aneurysm, effectively occluding the sac. The presence of the clot and subsequent endothelialization (formation of a new endothelial layer) over the coils promotes stabilization of the aneurysm, reducing the risk of rupture[7–9].

Coiling alters the flow dynamics within the aneurysm, resulting in a reduction in wall shear stress (WSS). High WSS has been associated with aneurysm growth and rupture. By disrupting the flow patterns and reducing the forces acting on the aneurysm wall, coiling helps decrease the WSS, which can contribute to the long-term stability of the aneurysm[10–13].

The presence of coils within the aneurysm initiates a healing response in the vessel wall. Over time, this can lead to positive remodeling, where the vessel wall thickens and strengthens around the coils. Positive remodeling reinforces the weakened aneurysm wall, enhancing its resistance to rupture. The presence of coils within the aneurysm provides a physical barrier that prevents the circulation of emboli (blood clots) from entering the cerebral circulation. This reduces the risk of thromboembolic events, which can further contribute to aneurysm rupture. Endovascular coiling, by altering the hemodynamics of the aneurysm, promotes flow diversion, aneurysm occlusion, and positive vessel remodeling[14–16]. These changes collectively contribute to the reduction in aneurysm rupture risk. However, it's important to note that the effectiveness of coiling can vary depending on

[1]Institute of Research and Development, Duy Tan University, Da Nang, Vietnam. [2]School of Engineering and Technology, Duy Tan University, Da Nang, Vietnam. [3]Faculty of Mechanical Engineering, University of Tabriz, Tabriz, Iran. [4]Petroleum Engineering Department, Faculty of Engineering, Soran University, Soran, Kurdistan Region 44008, Iraq. [5]Department of Chemical Engineering, University of Larestan, Larestan, Iran. ✉email: s.a_abdollahi@yahoo.com; saleh.o.hosseini95@gmail.com; sh850544@lar.ac.ir

factors such as aneurysm size, shape, and location. Patient-specific evaluation and careful consideration of the hemodynamic impact are crucial for successful treatment outcomes[17–20].

Endovascular coiling is a widely used treatment technique for intracranial aneurysms[21, 22]. While it can be effective for many aneurysms, the suitability of coiling as a treatment option depends on several factors, including the size and shape of the aneurysm. Endovascular coiling is commonly used for small to medium-sized aneurysms. Small aneurysms, typically defined as those with a maximum diameter less than 5 mm, are often ideal candidates for coiling due to their favorable outcomes and lower risk of rupture. Medium-sized aneurysms (5–15 mm) can also be treated with coiling, although the decision may depend on other factors such as the location and morphology of the aneurysm. Aneurysms come in various shapes, including saccular, fusiform, and irregular[23–26]. Saccular aneurysms with a well-defined neck and dome are generally more amenable to coiling. The presence of a narrow neck allows for better coil placement and stability within the aneurysm. Fusiform and irregular-shaped aneurysms, on the other hand, may present challenges for coiling due to their complex geometry and involvement of elongated segments. In such cases, alternative treatment options, such as flow diverters or surgical clipping, may be considered. The location of the aneurysm can also influence the feasibility of coiling. Aneurysms located in the anterior circulation, such as the anterior communicating artery or middle cerebral artery, are more commonly treated with coiling due to better accessibility and favorable outcomes. However, aneurysms in challenging locations, such as the posterior circulation or complex bifurcations, may pose technical difficulties for coiling[27–29].

It's important to note that the decision regarding the most appropriate treatment approach for an aneurysm is made on an individual basis, considering multiple factors such as aneurysm size, shape, location, patient's overall health, and the expertise of the treating physician[30–33]. In some cases, a combination of treatment techniques may be employed, such as using a flow diverter in conjunction with coiling or opting for surgical clipping for complex aneurysms. A multidisciplinary team, including neurosurgeons, interventional neuroradiologists, and neurologists, collaboratively assess each case to determine the most suitable treatment strategy for the patient's specific circumstances[34–37].

There are several scientific articles that present the hemodynamic analysis of the cerebral analysis via a computational approach. Unlike previous papers[38–41], in this paper, comprehensive investigations on the hemodynamics of the ICA aneurysm have been performed to disclose the effects of parent vessel mean diameter on the risk of aneurysm bleeding. The hemodynamic factors i.e. wall shear stress (WSS), oscillatory shear index (OSI), and pressure distribution on three different ICA cases have been developed and analyzed by computational fluid dynamic method. In addition, the influence of the endovascular coiling of the aneurysm on the blood flow characteristic is also revealed in the selected aneurysm.

Aneurysm selection and computational technique

For the selection of the aneurysm geometry, several rupture/un-rupture cerebral aneurysms have been obtained from the Aneurisk website[42] which contains geometrical features of the different patients from Emory University. It is confirming that all methods were carried out in accordance with relevant guidelines and regulations. Besides, all experimental protocols were approved by of the Ca' Granda Niguarda Hospital and it is confirmed that informed consent was obtained from all subjects and/or their legal guardian(s).

The three selected ICA aneurysms have different parent vessel mean diameters as presented in Table 1. As offered in Table 1, the size of the Parent vessel mean Diameter of the chosen cases is varied between 3.18 mm and 4.48 mm, and all cases are related to female patients. Table 1 also presents the HCT of the selected female patient and the sac section area. The size of the latter is in a limited range of (47–54 mm^2). Figure 1 displays the chosen saccular aneurysm with geometrical details.

The simulation of the blood flow is done via solving transient Navier–stocks equations while it is assumed that the blood flow is not Newtonian and the one-way FSI model is considered for the interactions of the vessel with the incoming blood stream[37]. Casson model is applied for the estimation of blood viscosity in our study[38, 39] and blood flow is considered laminar[40]. The applied boundary condition at the outlet and inlet is also displayed in Fig. 2. Two significant stages of peak systolic and early diastolic are also displayed in Fig. 2. The results of OSI are calculated.at the end of 3rd cardiac cycle of early diastolic as demonstrated in Fig. 2. The influence of the coiling is investigated by applying a porous domain in the sac section area with a porosity value of 0.844 as presented in Table 2.

The generated grid for the simulation of the blood flow on the selected cerebral aneurysm is displayed in Fig. 3. Efficient grid for numerical study is essential step[43–47]. The size of the grid on the vessel is almost uniform and the resolution of the produced grid on the cross-section of the parent vessel is higher in the vicinity of the aneurysm and vessel wall. As demonstrated in Fig. 3, the sac section region is split for applying the coiling porosity which is explained before. A close-up view is presented for the sac section area in the presented figure. To ensure the grid resolution, more than five grid sizes are produced and the average WSS on the sac section area

Case ID	Parent vessle mean diameter (mm)	Sac section area (mm^2)	Sex
16	3.18	47	Female (HCT = 0.40)
34	3.65	54	Female (HCT = 0.40)
38	4.48	50	Female (HCT = 0.40)

Table 1. Geometry details of selected aneurysms.

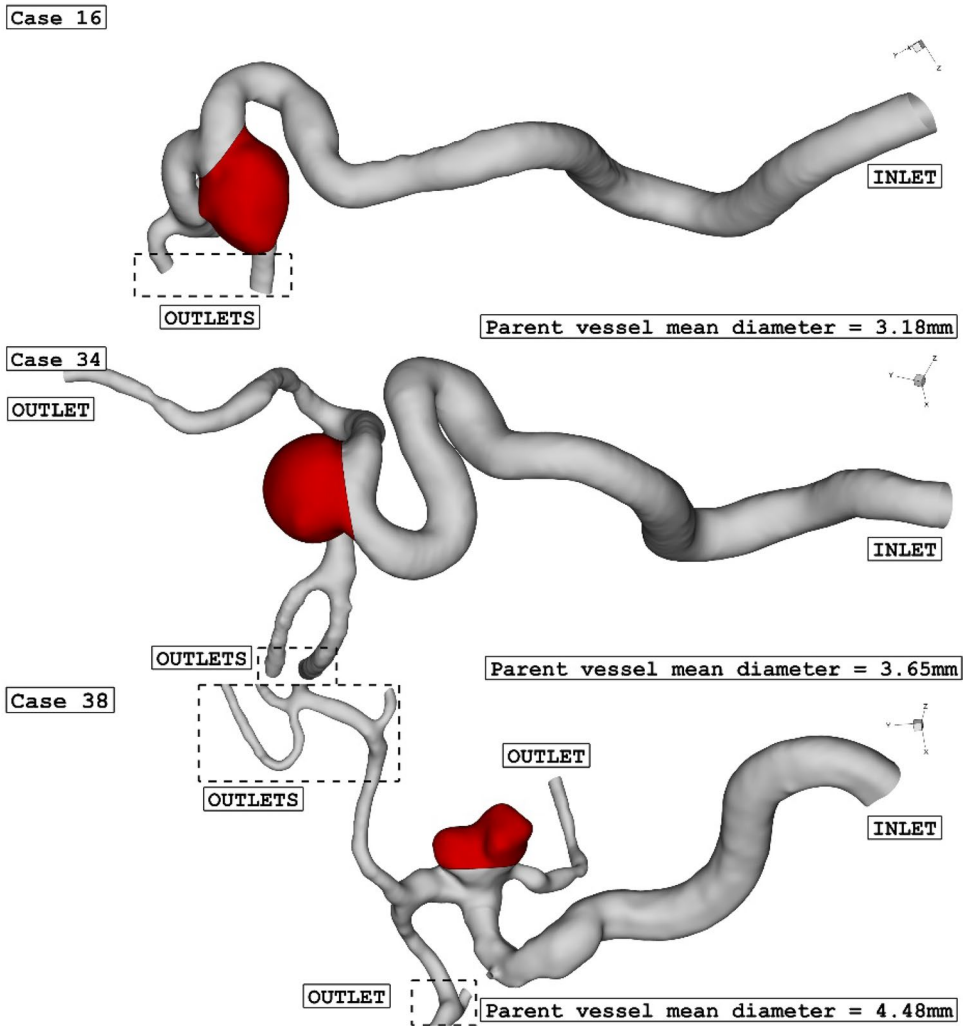

Figure 1. ICA aneurysm geometry of 3 different cases.

is calculated. Finally, the range of grid cells for the selected cases is within 1.1 million cells and 1.6 million cells. The using computational methodology for resolving real scientific problem is efficient and time consuming[48–50].

Results and conclusion

The details of hemodynamic factors related to the simulation of the aneurysms are presented in Table 3. In this table, the values of mean WSS, minimum WSS, OSI, wall pressure, and average velocity of the blood flow are reported. Except for OSI, all other factors are calculated for the peak systolic stage. In the following, the physical aspects of these achieved data are fully explained with a graphical contour.

The effects of the parent vessel's mean diameter on the mean WSS are demonstrated in Fig. 4. As plotted in Fig. 4, increasing parent vessel mean diameter considerably decreases the minimum WSS on sac surface. 80% reduction in mean WSS is attained at peak systolic when parent vessel mean diameter is increased about 40%. To recognize the effects of parent vessel mean diameter, Fig. 5 displays the WSS contour on sac area at peak systolic. Evaluation of WSS distribution indicates that the most critical area on the sac surface is neck section. In fact, in the neck section, the blood flow enters the sac and exit from sac with limited cross section area. The close-up view presents more details about the critical section in the neck section.

The variation of the mean sac wall pressure under impacts of different parent mean vessel are exhibited in Fig. 5. The figure shows that there is not a meaningful connection between the mean sac wall pressure and parent vessel mean diameter at peak systolic stage. Although, the change of parent vessel mean diameter in the chosen patients are high, the mean sac wall pressures varies restrictively. Figure 6 displays the changes of pressure contour on the sac surface in chosen models. In case 16, the maximum pressure is noticed in dome section while critical high pressure region happens near neck region in case 34. In case 38, neck region is critical from pressure aspects.

The changes of mean OSI for different parent vessel mean diameters are displayed in Fig. 7. The results show that increasing parent vessel mean diameter about 40% would decrease the mean OSI on the sac area about 43% at early diastolic. As demonstrated in Fig. 8, the most critical region for the rupture from OSI aspects is dome

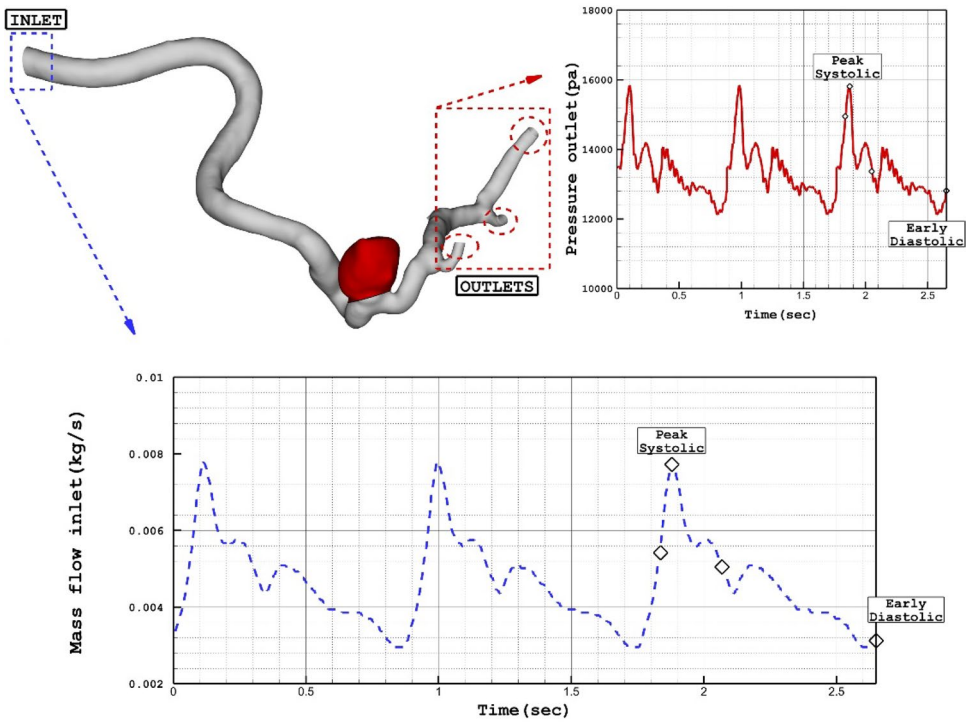

Figure 2. Applied mass and pressure profile at inlet and outlets.

HCT	Porosity	Viscous resistance (m2/1)
0.4	0.844	16,958,264.02

Table 2. Porosity of coiled aneurysms.

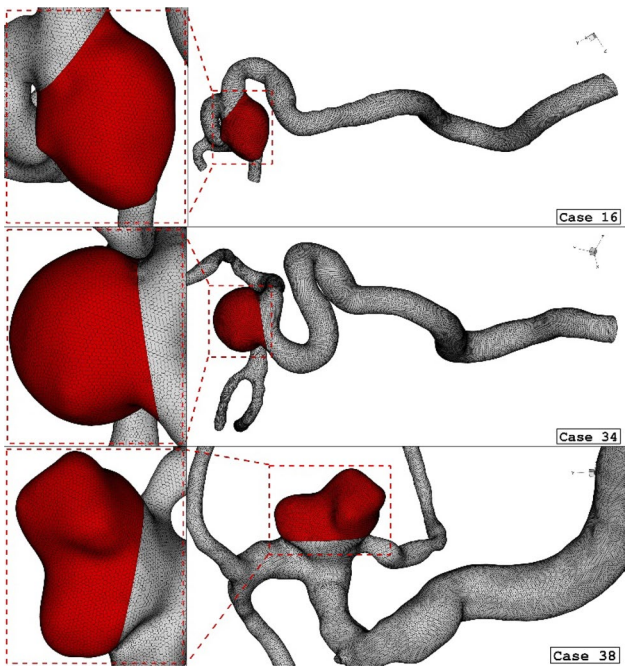

Figure 3. Grid generation for 3 different ICA cases.

	Parent vessel mean diameter (mm)	Sac section area (mm^2)	WSS_mean (Pa)	OSI_mean	Wall pressure_mean (Pa)	Aneurysm velocity_mean (m/s)
Case 16	3.18	47	9.368811	0.03234751	19,707.41	0.4137481
Case 34	3.65	54	8.146665	0.02603191	25,071.71	0.4034861
Case 38	4.48	50	2.778162	0.01463711	19,287.28	0.1811908

Table 3. Results of hemodynamic factors.

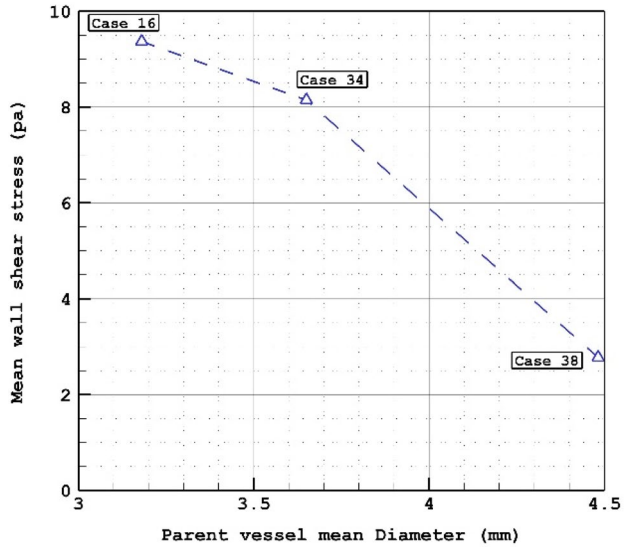

Figure 4. Mean wall shear stress versus parent vessel mean diameter at peak systolic.

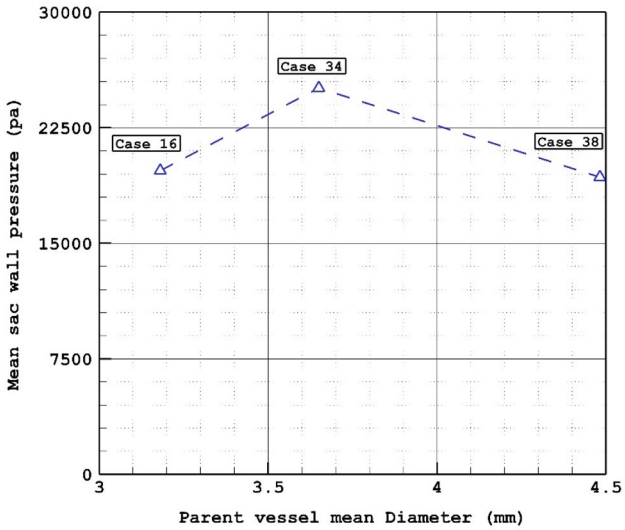

Figure 5. Mean wall pressure versus Parent vessel mean diameter at peak systolic.

region where has higher OSI value. It is also found that the maximum OSI value on the dome area is also reduced from 0.35 to 0.15 by increasing the diameter of the parent vessel.

Figure 9 illustrates the impacts of parent vessel mean diameter on the mean velocity inside the sac region. As demonstrated in Fig. 10, 44% reduction in mean velocity of the blood velocity is noticed as 41% increase in parent vessel mean diameter is observed. The structure of the blood flow inside the cerebral aneurysm is compared for the selected patients by demonstrating the iso-velocity contour in Fig. 10. The structure of the iso-velocity

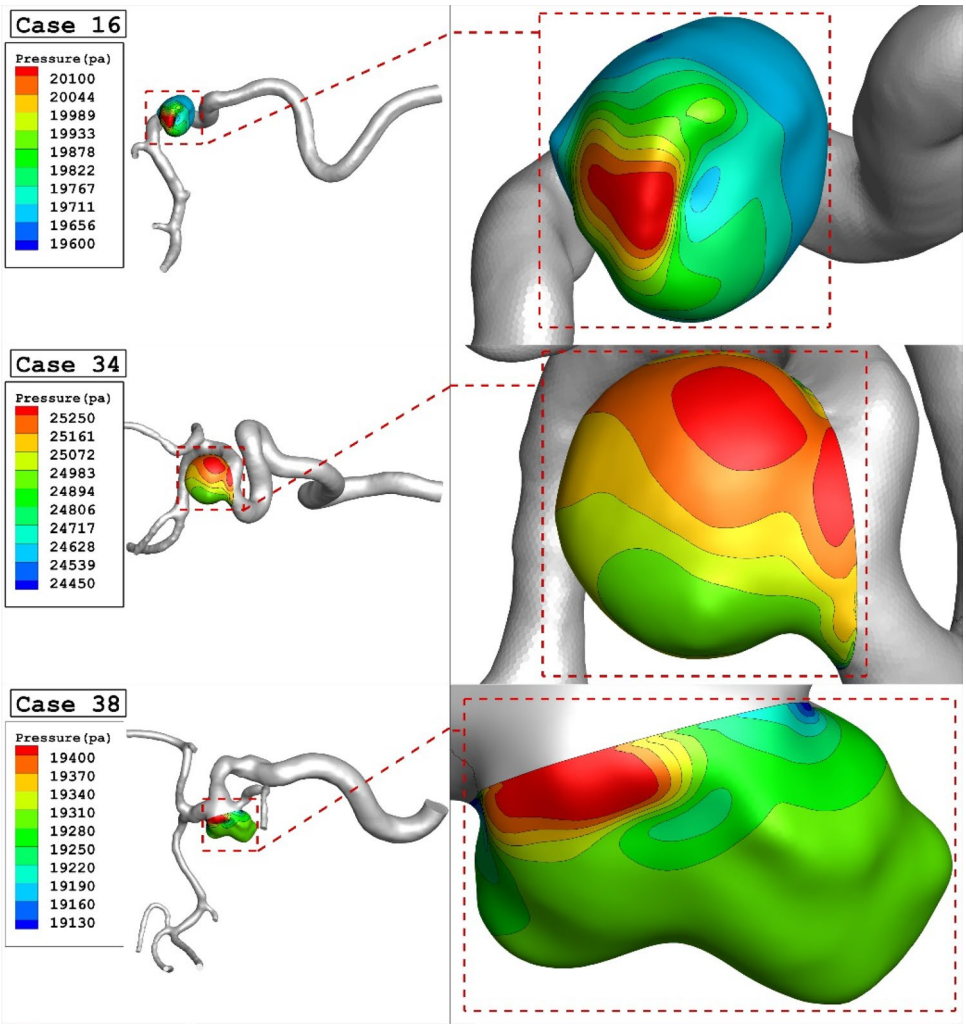

Figure 6. Wall pressure contours (Peak systolic) in different cases.

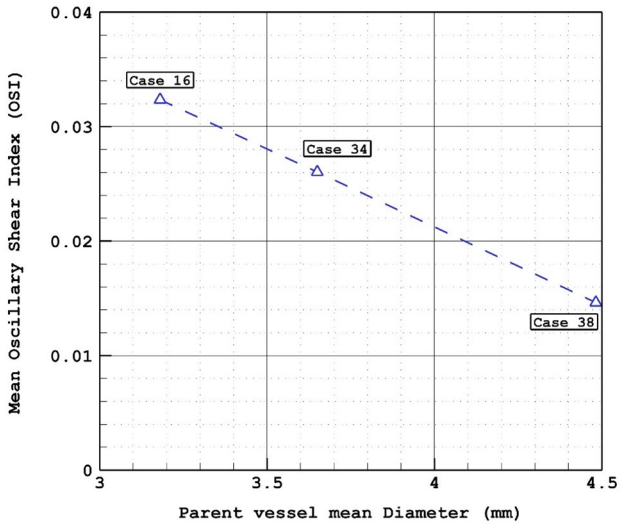

Figure 7. Mean OSI versus Parent vessel mean diameter at early diastolic.

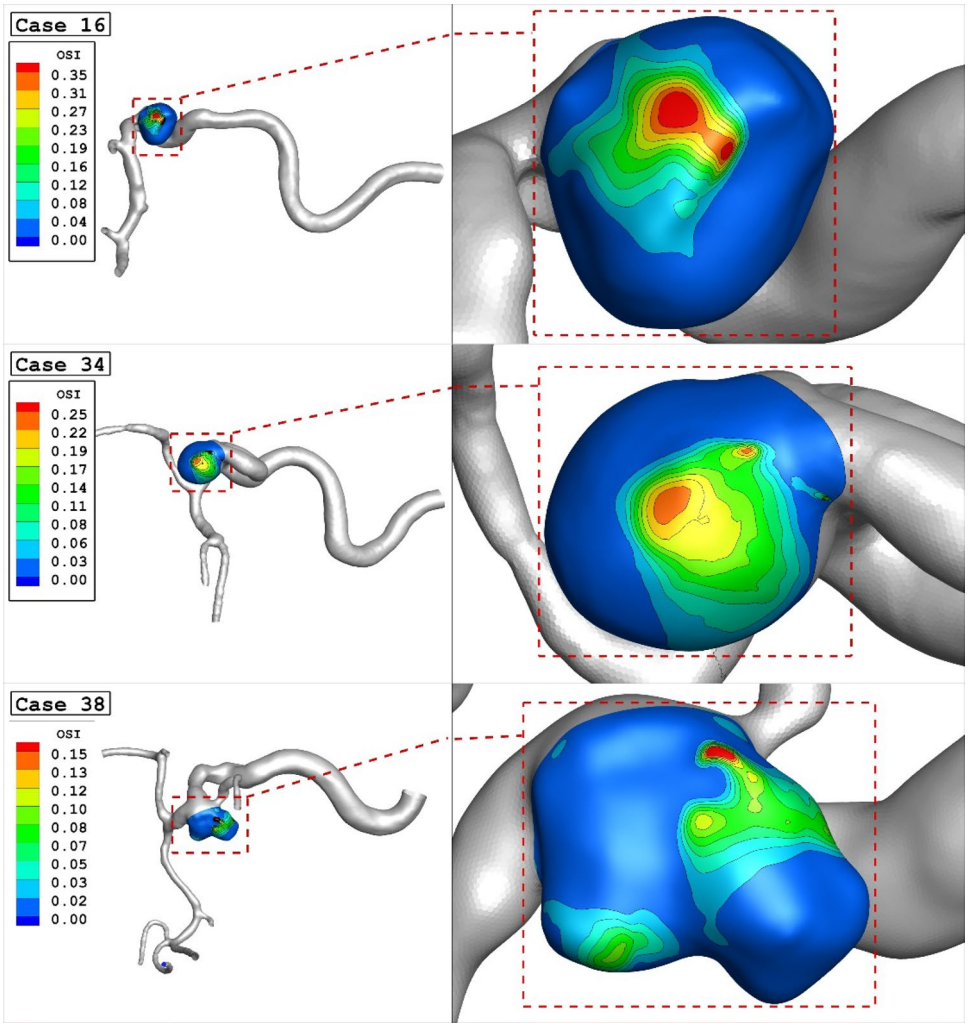

Figure 8. OSI contours (Early diastolic) in different cases.

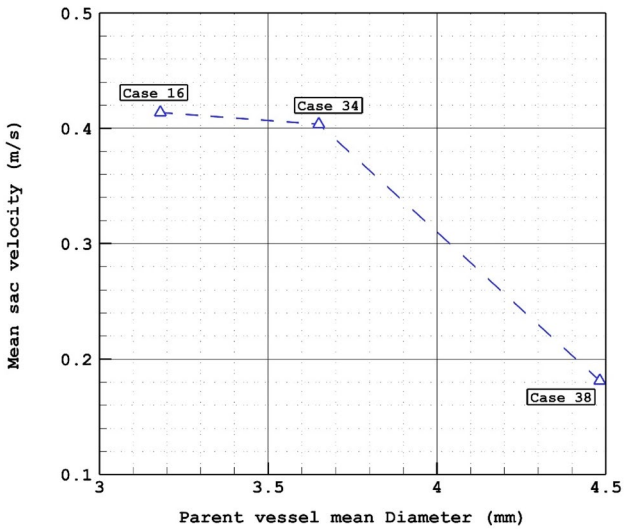

Figure 9. Mean sac velocity versus Parent vessel mean diameter at peak systolic.

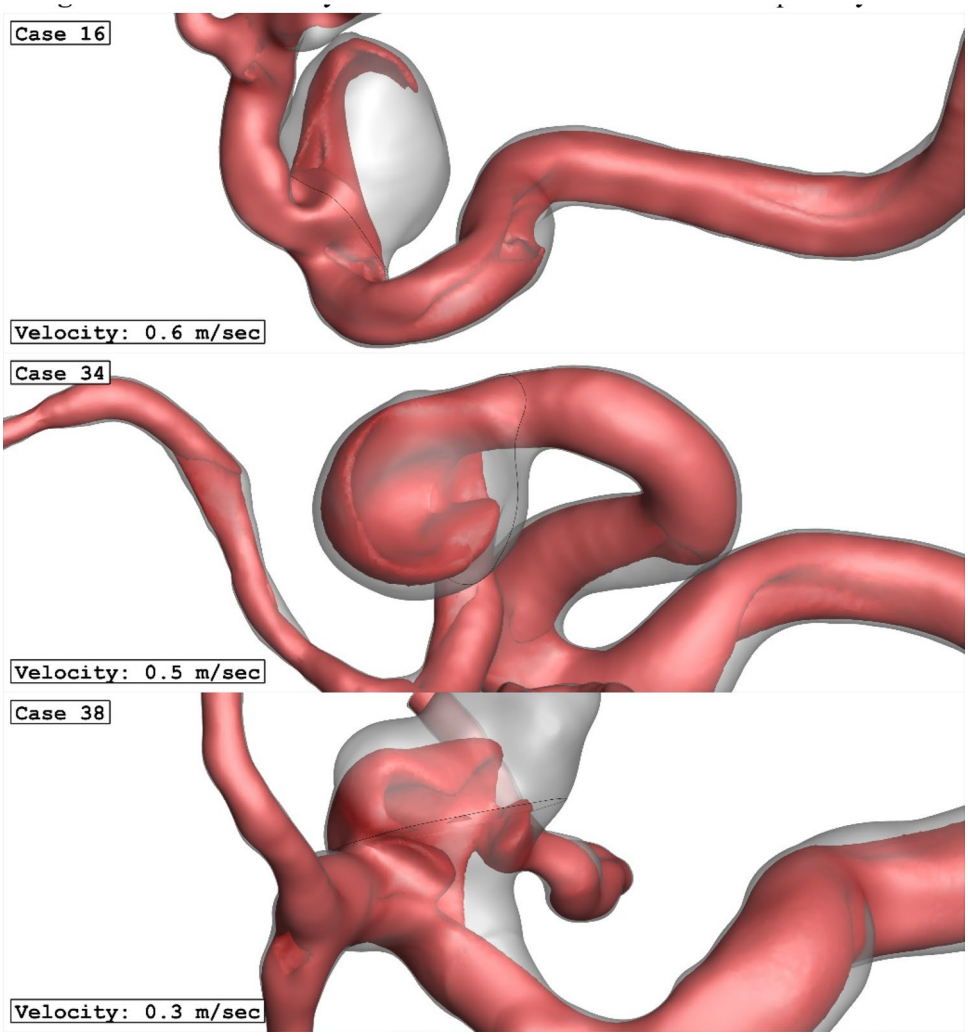

Figure 10. Iso-Surface (velocity at peak systolic) in different cases.

indicates that the velocity in center of the aneurysm is less than other region and the shape of aneurysm is very important on the feature of blood flow.

Conclusion

The present study has focused on the impacts of the parent vessel mean diameter on the hemodynamic aspects of the cerebral aneurysm with endovascular coiling. Computational approach is used to model the transient blood flow inside the parent vessel and sac area while it is presumed that the blood is not Newtonian fluid. The contours of pressure, WSS and OSI of three nominated ICA aneurysms are compared to disclose the importance of the parent vessel mean diameter on the probability of aneurysm bleeding. Based on the OSI results at early diastolic, increasing parent vessel mean diameter about 40% would decrease the mean OSI on the sac area about 43%.

Data availability

All data generated or analysed during this study are included in this published article.

Received: 5 November 2023; Accepted: 23 November 2023
Published online: 25 November 2023

References

1. Sadeh, A. *et al.* Computational study of blood flow inside MCA aneurysm with/without endovascular coiling. *Sci. Rep.* **13**, 4560. https://doi.org/10.1038/s41598-023-31522-x (2023).
2. Zhang, Z. *et al.* Endoscope image mosaic based on pyramid ORB. *Biomed. Signal Process. Control* **71**, 103261. https://doi.org/10.1016/j.bspc.2021.103261 (2022).
3. Liu, Y. *et al.* Improved feature point pair purification algorithm based on SIFT during endoscope image stitching. *Front. Neurorobot.* https://doi.org/10.3389/fnbot.2022.840594 (2022).

4. Jin, H. & Wang, Z. Boundedness, blowup and critical mass phenomenon in competing chemotaxis. *J. Differ. Equ.* **260**(1), 162–196. https://doi.org/10.1016/j.jde.2015.08.040 (2016).
5. Shan, Y. *et al.* Evidence of a large current of transcranial alternating current stimulation directly to deep brain regions. *Mol. Psychiatry* https://doi.org/10.1038/s41380-023-02150-8 (2023).
6. Lu, S., Yang, J. & Yin, B. Analysis and design of surgical instrument localization algorithm. *Comput Model Eng Sci* **137**(1), 669–685. https://doi.org/10.32604/cmes.2023.027417 (2023).
7. Ye, X., Wang, J., Qiu, W., Chen, Y. & Shen, L. Excessive gliosis after vitrectomy for the highly myopic macular hole: A Spectral domain optical coherence tomography study. *RETINA* https://doi.org/10.1097/IAE.0000000000003657 (2023).
8. Gao, Z. *et al.* Automatic interpretation and clinical evaluation for fundus fluorescein angiography images of diabetic retinopathy patients by deep learning. *Brit. J. Ophthalmol.* https://doi.org/10.1136/bjo-2022-321472 (2022).
9. Zhao, J. *et al.* Heart–gut microbiota communication determines the severity of cardiac injury after myocardial ischaemia/reperfusion. *Cardiovasc. Res.* **119**(6), 1390–1402. https://doi.org/10.1093/cvr/cvad023 (2023).
10. Chen, Y., Chen, L. & Zhou, Q. Genetic association between eNOS gene polymorphisms and risk of carotid atherosclerosis A meta-analysis. *Herz* **46**(2), 253–264. https://doi.org/10.1007/s00059-020-04995-z (2021).
11. Huang, A. & Zhou, W. Mn-based cGAS-STING activation for tumor therapy. *Chin. J. Cancer Res.* **35**(1), 19–43. https://doi.org/10.21147/j.issn.1000-9604.2023.01.04 (2023).
12. Sabernaeemi, A. *et al.* Influence of stent-induced vessel deformation on hemodynamic feature of bloodstream inside ICA aneurysms. *Biomech. Model Mechanobiol.* https://doi.org/10.1007/s10237-023-01710-9 (2023).
13. Salavatidezfouli, S. *et al.* Investigation of the stent induced deformation on hemodynamic of internal carotid aneurysms by computational fluid dynamics. *Sci. Rep.* **13**(1), 7155 (2023).
14. Salavatidezfouli, S. *et al.* Investigation of the stent induced deformation on hemodynamic of internal carotid aneurysms by computational fluid dynamics. *Sci. Rep.* **13**, 7155 (2023).
15. Poueinak, M. M. *et al.* Computational study of blood hemodynamic in ICA aneurysm with coiling embolism. *Int. J. Modern Phys. C* **34**(6), 2350138. https://doi.org/10.1142/S0129183123501383 (2023).
16. Hariri, S., Poueinak, M. M., Hassanvand, A., Barzegar Gerdroodbary, M. & Faraji, M. Effects of blood hematocrit on performance of endovascular coiling for treatment of middle cerebral artery (MCA) aneurysms: Computational study. *Interdiscip. Neurosurg.* **32**, 101729 (2023).
17. Jin, Z.-H., Barzegar Gerdroodbary, M., Valipour, P., Faraji, M. & Abu-Hamdeh, N. H. CFD investigations of the blood hemodynamic inside internal cerebral aneurysm (ICA) in the existence of coiling embolism. *Alex. Eng. J.* https://doi.org/10.1016/j.aej.2022.10.070 (2023).
18. Sheidani, A. *et al.* Influence of the coiling porosity on the risk reduction of the cerebral aneurysm rupture: Computational study. *Sci. Rep.* **12**, 19082. https://doi.org/10.1038/s41598-022-23745-1 (2022).
19. Sadeh, A., Kazemi, A., Bahramkhoo, M., Barzegar Gerdroodbary, M. Computational analysis of the blood hemodynamic inside internal cerebral aneurysm in the existence of endovascular coiling. *Int. J. Modern Phys. C* 2350059 (2022).
20. Wang, Y. *et al.* Rhubarb attenuates blood-brain barrier disruption via increased zonula occludens-1 expression in a rat model of intracerebral hemorrhage. *Exp. Ther. Med.* **12**(1), 250–256. https://doi.org/10.3892/etm.2016.3330 (2016).
21. Mao, X. *et al.* Tissue resident memory T cells are enriched and dysfunctional in effusion of patients with malignant tumor. *J. Cancer* **14**(7), 1223–1231. https://doi.org/10.7150/jca.83615 (2023).
22. Liang, X. *et al.* Comparative study of microvascular structural changes in the gestational diabetic placenta. *Diabetes Vasc. Dis. Res.* **20**(3), 1497016315. https://doi.org/10.1177/14791641231173627 (2023).
23. Chen, S. *et al.* RNA adenosine modifications related to prognosis and immune infiltration in osteosarcoma. *J. Transl. Med.* **20**(1), 228. https://doi.org/10.1186/s12967-022-03415-6 (2022).
24. He, B. *et al.* A machine learning framework to trace tumor tissue-of-origin of 13 types of cancer based on DNA somatic mutation. *Biochim. Biophys. Acta BBA Mol. Basis Dis.* **1866**(11), 165916. https://doi.org/10.1016/j.bbadis.2020.165916 (2020).
25. Xu, B. *et al.* Identification of key genes in ruptured atherosclerotic plaques by weighted gene correlation network analysis. *Sci. Rep.* **10**(1), 10847. https://doi.org/10.1038/s41598-020-67114-2 (2020).
26. Huang, H. *et al.* The behavior between fluid and structure from coupling system of bile, bile duct, and polydioxanone biliary stent: A numerical method Med. *Eng. Phys.* **113**, 103966. https://doi.org/10.1016/j.medengphy.2023.103966 (2023).
27. Zhou, L. *et al.* The SNHG1-centered ceRNA network regulates cell cycle and is a potential prognostic biomarker for hepatocellular carcinoma. *Tohoku J. Exp. Med.* **258**(4), 265–276. https://doi.org/10.1620/tjem.2022.J083 (2022).
28. Tateshima, S. *et al.* Three-dimensional blood flow analysis in a wide necked internal carotid artery-ophthalmic artery aneurysm. *J. Neurosurg.* **99**, 526–533 (2003).
29. Valipour, P. Effects of coiling embolism on blood hemodynamic of the MCA aneurysm: A numerical study. *Sci. Rep.* **12**(1), 22029 (2022).
30. Steinman, D. A., Milner, J. S., Norley, C. J., Lownie, S. P. & Holdsworth, D. W. Image-based computational simulation of flow dynamics in a giant intracranial aneurysm. *Am. J. Neuroradiol.* **24**, 559–566 (2003).
31. Chatziprodromou, I., Butty, V., Makhijani, V. B., Poulikakos, D. & Ventikos, Y. Pulsatile blood flow in anatomically accurate vessels with multiple aneurysms: A medical intervention planning application of computational haemodynamics. *Flow Turbul. Combust.* **71**, 333–346 (2003).
32. Shen, X.-Y., Barzegar Gerdroodbary, M., Abazari, A. M. & Moradi, R. Computational study of blood flow characteristics on formation of the aneurysm in internal carotid artery. *Eur. Phys. J. Plus* **136**(5), 541 (2021).
33. Shen, X.-Y. *et al.* Numerical simulation of blood flow effects on rupture of aneurysm in middle cerebral artery. *Int. J. Modern Phys. C* **33**(03), 2250030 (2022).
34. Rostamian, A., Fallah, K., Rostamiyan, Y., Alinejad, J. Application of computational fluid dynamics for detection of high risk region in middle cerebral artery (MCA) aneurysm. *Int. J. Modern Phys. C* 2350019 (2022).
35. Qin, S. *et al.* Efficient parallel simulation of hemodynamics in patient-specific abdominal aorta with aneurysm. *Comput. Biol. Med.* **136**, 104652 (2021).
36. Xu, L., Liang, F., Zhao, B., Wan, J. & Liu, H. Influence of aging-induced flow waveform variation on hemodynamics in aneurysms present at the internal carotid artery: A computational model-based study. *Comput. Biol. Med.* **101**, 51–60 (2018).
37. Boccadifuoco, A., Mariotti, A., Celi, S., Martini, N. & Salvetti, M. V. Impact of uncertainties in outflow boundary conditions on the predictions of hemodynamic simulations of ascending thoracic aortic aneurysms. *Comput. Fluids* **165**, 96–115 (2018).
38. Mitsos, A. P., Kakalis, N. M. P., Ventikos, Y. P. & Byrne, J. V. Haemodynamic simulation of aneurysm coiling in an anatomically accurate computational fluid dynamics model. *Neuroradiology* **50**(4), 341–347 (2008).
39. Valencia, A., Morales, H., Rivera, R., Bravo, E. & Galvez, M. Blood flow dynamics in patient-specific cerebral aneurysm models: The relationship between wall shear stress and aneurysm area index. *Med. Eng. Phys.* **30**, 329–340 (2008).
40. Fung, Y. C. *Biomechanics: Mechanical Properties of Living Tissues* 2nd edn. (Springer, 1993).
41. Razavi, A., Shirani, E. & Sadeghi, M. Numerical simulation of blood pulsatile flow in a stenosed carotid artery using different rheological models. *J. Biomech.* **44**, 2021–2030 (2011).
42. AneuriskWeb project website, http://ecm2.mathcs.emory.edu/aneuriskweb. Emory University, Department of Math&CS, (2012).
43. Othman, G. Q., Saeed, R. S., Kadir, D. H. & Taher, H. J. Relation of angiography to hematological, hormonal and some biochemical variables in coronary artery bypass graft patients. *J. Phys. Conf. Ser.* **1294**(6), 062110 (2019).

44. Hu, H., Luo, P., Kadir, D. H., Hassanvand, A. Assessing the impact of aneurysm morphology on the risk of internal carotid artery aneurysm rupture: A statistical and computational analysis of endovascular coiling. *Phys. Fluids* 35(10) (2023).
45. Zhou, L., Kadir, D. H., Shi, L., Mousavi, S. V., Huang, X. The influence of aneurysm feature on coiling treatment of internal carotid artery aneurysms: Numerical and statistical study. *Int. J. Modern Phys. C* 2450031 (2023)
46. Yang, J., Kadir, D. H. Data mining techniques in breast cancer diagnosis at the cellular–molecular level. *J. Cancer Res. Clin. Oncol.* 1–16 (2023).
47. Sadeghi, A., Amini, Y., Saidi, M. H. & Yavari, H. Shear-rate-dependent rheology effects on mass transport and surface reactions in biomicrofluidic devices. *AIChE J* **61**(6), 1912–1924 (2015).
48. Farahnakian, M., Keshavarz, M. E., Elhami, S. & Razfar, M. R. Effect of cutting edge modification on the tool flank wear in ultrasonically assisted turning of hardened steel. *Proc Inst Mech Eng Part B J Eng Manuf* **233**(5), 1472–1482 (2019).
49. Farahnakian, M., Razfar, M. R. & Biglari, F. R. Multi-constrained optimization in ultrasonic-assisted turning of hardened steel by electromagnetism-like algorithm. *Proc Inst Mech Eng Part B J Eng Manuf* **229**(11), 1933–1944 (2015).
50. Jiang, H., Lu, Z., Barzegar Gerdroodbary, M., Sabernaeemi, A. & Salavatidezfouli, S. The influence of sac centreline on saccular aneurysm rupture: computational study. *Sci. Rep.* **13**(1), 11288 (2023).

Author contributions

M.F. and S.A.A. wrote the main manuscript text and A.H.A and S.H. prepared figures and P.D. supervised the project. All authors reviewed the manuscript.

Competing interests

The authors declare no competing interests.

Additional information

Correspondence and requests for materials should be addressed to S.A.A. or S.H.

Reprints and permissions information is available at www.nature.com/reprints.

Publisher's note Springer Nature remains neutral with regard to jurisdictional claims in published maps and institutional affiliations.